Dynamic Tuning of Sensitivity and Bandwidth of High-Q Transducers via Nested Phase Modulations

Aidan Fitzpatrick*, Ajay Singhvi*, and Amin Arbabian
Department of Electrical Engineering, Stanford University, Stanford, CA, USA

2022 IEEE International Symposium on Circuits and Systems (ISCAS) | 978-1-6654-8485-5/22/$31.00 ©2022 IEEE | DOI: 10.1109/ISCAS48785.2022.9937917

***Abstract*—Non-contact and long-range acoustic or multi-modal sensing in air can be employed for a number of industrial, IoT, biomedical, and remote-sensing applications but requires the use of resonant, highly sensitive ultrasonic receivers to achieve sufficient SNR. Fabrication of such resonant MEMS sensors fundamentally trades off bandwidth for sensitivity, thus limiting resolution in these sensing systems. In this paper, we devise an all-electronic means of dynamically tuning the sensitivity and bandwidth of high quality factor sensors by using a nested phase modulation scheme that simultaneously achieves high bandwidth and high SNR. We demonstrate an $> 8\times$ increase in bandwidth in ultrasonic ranging and non-contact photoacoustic measurements, while concurrently boosting the SNR by up to $13\times$ with potential for further enhancement.**

***Index Terms*—Air-coupled, Bandwidth, CMUT, High-Q, Non-Contact Sensing, Phase Modulation, Photoacoustic, Resonant, Sensitivity, Thermoacoustic, Ultrasound**

I. Introduction

Air-coupled ultrasound (US) is employed for many applications including non-destructive testing [1]–[3], close-proximity object detection [4]–[6], and human-computer interaction [7]–[9]. In addition, air-coupled US detection has enabled non-contact thermoacoustic/photoacoustic (TA/PA) imaging for applications such as underground root imaging [10], underwater imaging [11], as well as biomedical imaging [12].

Inevitably, dispersion and atmospheric absorption of sound attenuates airborne acoustic signals and thus fundamentally constrains the maximum detection range of such air-coupled US systems [7]. Furthermore, the non-contact applications suffer an additional large interface loss as the acoustic signals propagate from the imaged medium into the air [13]. As a result, it is of paramount importance that the receiving transducer is able to detect weak acoustic signals, or have high receive sensitivity, in order to push the detection limits.

Capacitive micromachined ultrasonic transducers (CMUTs) are MEMS based sensors that offer high electromechanical coupling and thus high receive sensitivity among other advantages related to fabrication and device integration [14]–[16]. Fabricated using thin vibrating plates, CMUTs have an acoustic impedance that is well-matched to air and thus operate as very efficient air-coupled transducers [17], [18]. Like other sensors though, they are constrained by an inherent sensitivity-bandwidth tradeoff.

Previous works introduce various damping mechanisms to achieve an application-specific desired transducer bandwidth at the cost of a considerable reduction in sensitivity [17]–[19]. Recently though, as illustrated in Fig. 1**a-b**, Ma *et al.* introduced a multi-parameter optimization method to achieve a near constant sensitivity-bandwidth product as a function of their primary design knob – the height of trenches etched in the substrate of the CMUT [14]. One of the underlying limitations of introducing damping to achieve a desired bandwidth, in addition to a loss of sensitivity, is that the chosen operation point within this tradeoff space is fixed by the geometric design decisions.

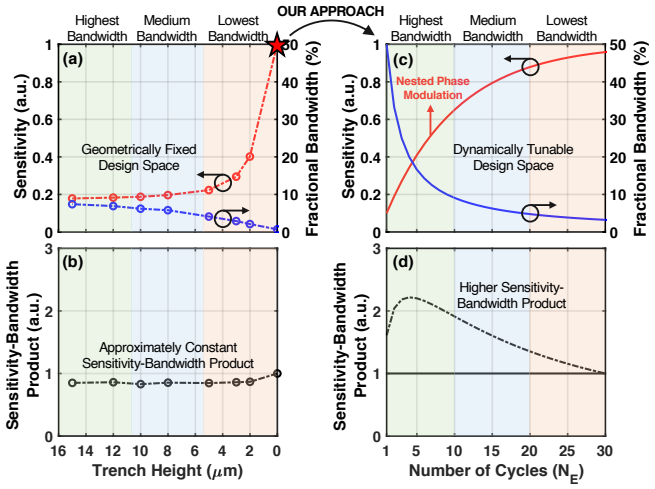

Fig. 1. (a) Sensitivity versus bandwidth tradeoff and (b) Sensitivity-bandwidth product for geometrically fixed transducer designs [14]. (c) Sensitivity versus bandwidth tradeoff and (d) Sensitivity-bandwidth product using the proposed technique in this work.

Our proposed approach, as shown in Fig. 1, is to utilize a highly resonant transducer that is optimized for sensitivity and instead exploit a signal encoding scheme to tune bandwidth. Previous work introduced a coded excitation scheme that demonstrated simulations with increased resolution despite using highly resonant transducers [20]. As we will show, this technique permits dynamically tuning across the sensitivity-bandwidth tradeoff space shown in Fig. 1**c** – allowing a fixed transducer design to be flexible to various application requirements. In fact, this approach also demonstrates fractional bandwidths much beyond those achieved in [14] and does so while exceeding the sensitivity-bandwidth product (Fig. 1**d**).

In this work, we operate the CMUT in the highest bandwidth regime depicted in Fig. 1**c** such that large fractional bandwidths can be achieved. We introduce a nested phase modulated waveform in which the aforementioned coded excitation is embedded within a binary phase sequence; this

This work was supported by Advanced Research Projects Agency-Energy Grant DE-AR0000825.
*A. Fitzpatrick and A. Singhvi contributed equally to this work.

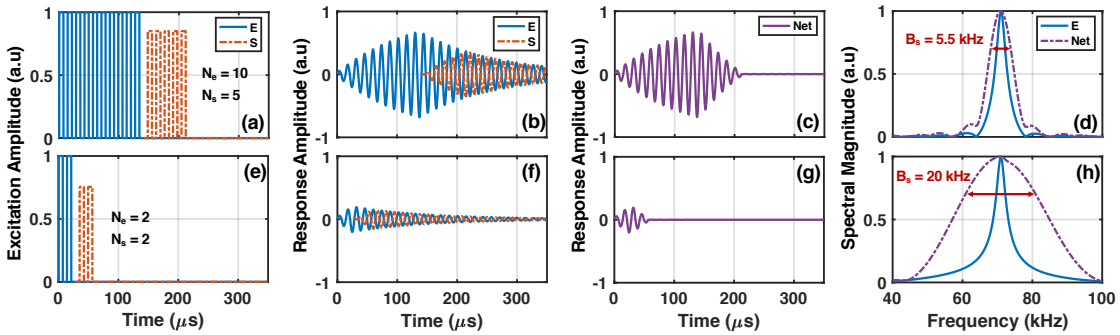

Fig. 2. (a) Transmitted signal, (b) receiver response, (c) net signal, (d) and spectrum using the coded pulse scheme with 10 excitation (E) cycles ($N_e = 10$) and 5 suppression (S) cycles ($N_s = 5$). (e) Transmitted signal, (f) receiver response, (g) net signal, (h) and spectrum using the coded pulse scheme with 2 excitation cycles and 2 suppression cycles.

technique compensates for degradation in sensitivity with signal processing gains. Lastly, we demonstrate the efficacy of the proposed nested phase modulated waveform experimentally for both airborne US ranging and non-contact TA/PA applications.

II. System Metrics

Arguably the two most fundamental metrics that quantify the performance of sensing and imaging systems are the resolution at which targets can be distinguished and the signal-to-noise ratio (SNR), which is often the primary constraint on the maximum detection range. Herein, mentions of resolution will refer specifically to range resolution. Unfortunately, SNR is dependent on the receiver sensitivity and resolution is dependent on the bandwidth, thus achieving high resolution and high SNR are conflicting objectives due to the sensitivity versus bandwidth tradeoff.

Before discussing these objectives, it is important to differentiate between the airborne acoustic wave incident on the receiver and the received electrical signal that is passed to the signal processing pipeline. Let $i(t)$ be an airborne acoustic wave that is incident on a receiver with impulse response $h(t)$. The receiver can be thought of as a linear, time-invariant filter with some gain (i.e. sensitivity) and bandwidth B_{rec}, such that the received signal is $s(t) = i(t) * h(t) + n(t)$ where $*$ denotes the convolution operator and $n(t)$ is additive noise. As will be shown, it is ultimately the characteristics of the received electrical signal, including its average power P_s and bandwidth B_s, that determine system performance.

Invoking a far-field approximation, the range resolution (S_r) of a sensing system is inversely proportional to B_s with the well-known relationship [21]:

$$S_r = \frac{c}{2B_s}, \tag{1}$$

where c is the speed-of-sound and the factor of 2 in the denominator is due to the two-way propagation. It is noteworthy that this factor would be dropped for TA/PA imaging due to the one-way acoustic propagation. Therefore, to improve resolution, or achieve a smaller S_r, a system designer may aim to increase B_s by transmitting broadband signals and using broadband transducers (wider B_{rec}).

The caveat here, as depicted in Fig. 1**a**, is that broadband transducers tradeoff sensitivity for bandwidth. Assuming the use of a matched filter in the receiver chain, which can be employed for optimal SNR, the peak instantaneous SNR of the matched filter output at the time-of-arrival of the received signal-of-interest is [21]:

$$SNR(t_{TOA}) = \frac{2E_s}{N_0} = \frac{2P_s\tau_p}{N_0}, \tag{2}$$

where E_s and τ_p are the energy and temporal duration, or pulse width, of the signal-of-interest, and where $N_0/2$ is the white noise power spectral density of the receiver system which incorporates both the mechanical noise of the transducer as well as the additive noise from the receiver electronics.

Since the power in the received signal P_s is proportional to the receiver's sensitivity, increasing B_{rec} degrades SNR accordingly. In addition to loss in receiver sensitivity, it is also fundamental that a transducer's mechanical noise is a function of its bandwidth; as losses, such as damping mechanisms, are introduced to effectively widen B_{rec}, the transducer's noise floor increases considerably [14]. Consequently, resonant transducers are typically used – despite sacrificing resolution – to maximize sensitivity to the weak acoustic signals in airborne US ranging and in non-contact TA/PA applications [4], [13].

As discussed in the next section, our goal is to exploit the fact that the resolution is dependent on B_s whereas the SNR has higher dependence on B_{rec} to establish a means for achieving $B_s >> B_{rec}$ and thus high SNR and high resolution with a resonant transducer.

III. Waveform Design

A. Coded Pulse Scheme

Previous work developed a coded pulse excitation scheme that showed simulations with increased resolution despite operating with resonant transducers [20]. The basis of this concept is depicted in Fig. 2. For the illustrated simulations, the transducer is modeled as a second order transfer function with a 71 kHz resonance frequency and a high quality factor (Q) of 28 or equivalently a B_{rec} of 2.5 kHz; this models the characteristics of the transducer used in later experiments.

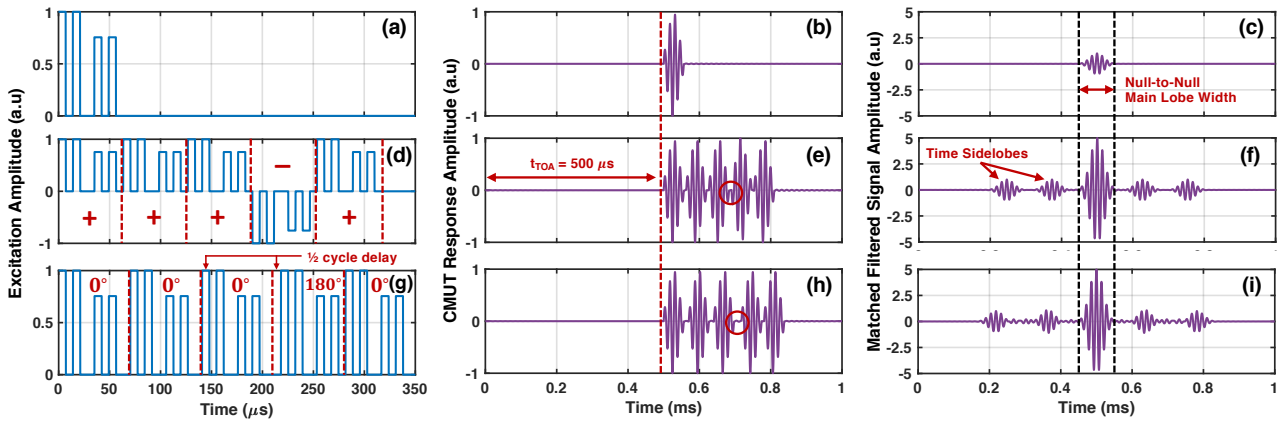

Fig. 3. (a) Transmitted 1-symbol waveform, (b) Transducer response to waveform in (a), (c) Matched filtered signal in (b). (d) Transmitted 5-symbol waveform, (e) Transducer response to waveform in (d), (f) Matched filtered signal in (e). (g) Transmitted 5-symbol waveform using only positive modulation, (h) Transducer response to waveform in (g), Matched filtered signal in (h).

A typical transmit signal for such a high-Q transducer may consist of a number of excitation pulses (N_e) at the transducer's resonance frequency (Fig. 2**a**). The transducer's response to this will include a ringing up in amplitude for each additional pulse (saturates as $N_e \rightarrow Q$) as well as a ringing down in amplitude after the excitation pulses conclude (Fig. 2**b**). The ring down time or tail of this response is due to the limited B_{rec} and inherently reduces resolution as subsequently received signals could be overlapping and occluded.

To eliminate the tail of the received signal, a number of suppression pulses (N_s) can follow the excitation (Fig. 2**a**); if the suppression pulses are appropriately time-shifted and scaled [20], the tail can be effectively canceled out such that the received signal has reduced temporal duration (Fig. 2**c**) and thus increased B_s (Fig. 2**d**). The increase in B_s is even more pronounced as the number of excitation pulses is reduced (Fig. 2**h**) – albeit at the cost of signal amplitude (Fig. 2**g**).

The loss in signal amplitude noted when using fewer excitation pulses is a result of not ringing the transducer up to its full sensitivity and thus can be thought of a degradation in sensitivity. The tradeoff between B_s and sensitivity as a function of the number of excitation pulses when using this coded excitation scheme is shown in Fig. 1**c**. The key takeaways of this signal encoding technique are as follows: 1) using a single transducer, the desired operation point in the sensitivity versus bandwidth tradeoff space can be dynamically tuned to meet application requirements by simply modifying the transmit signal; 2) whereas an N-times increase in bandwidth can be achieved with an N-times decrease in sensitivity (i.e. constant sensitivity-bandwidth product) for geometrically tuned transducers (Fig. 1**b**), this technique enables increasing bandwidth with lesser sacrifice in sensitivity (Fig. 1**d**); and 3) $B_s >> B_{rec}$ can be achieved for increasing resolution in applications where resolution may be critical.

Despite the improvement in sensitivity-bandwidth product using this technique, there is still some degradation in sensitivity as B_s is increased. In the next section, we articulate how the high bandwidth coded excitation can be nested within a phase modulated waveform such that high resolution and high SNR can be simultaneously achieved with resonant transducers.

B. Nested Phase Modulation

Strategically modulated pulses, such as frequency or phase modulations, enable increasing the energy in the transmit signal such that the matched filtered received signal has higher SNR [21]. For phase modulation, a pulse of length τ_p can be subdivided into N symbols of length τ_s where $\tau_s = \tau_p/N$. If the phase of each symbol is chosen appropriately and a matched filter is employed, resolution will be dictated by the bandwidth of the symbol of length τ_s whereas the SNR will be dictated by the energy in the total pulse of length τ_p [22].

In Section II, we reviewed a coded excitation scheme that enables $B_s >> B_{rec}$ such that resolution is enhanced. Here, we demonstrate that a shorter, high bandwidth coded excitation of length τ_s can be a single symbol nested within a phase modulated waveform of length τ_p.

A single coded pulse symbol with $N_e = 2$ is shown in Fig. 3**a** with the corresponding simulated transducer response, or received signal, shown in Fig. 3**b** assuming $t_{TOA} = 500\ \mu s$. The matched filter output for this signal is shown in Fig. 3**c**. If this symbol is nested in a binary phase code of length $N = 5$ with a phase sequence of (0°, 0° , 0°, 180°, 0°) or equivalently an amplitude scaling of (+1, +1, +1, -1, +1), as shown in Fig. 3**d**, the received signal will be that shown in Fig. 3**e**.

While it appears that the longer transducer response would occlude subsequently received signals, the matched filter compresses the longer pulse into a short pulse (Fig. 3**f**). Note that the compressed pulse has a main lobe width equivalent to that of the single symbol therefore achieving equivalent resolution, but with N-times greater SNR. The utilized code belongs to a family of binary phase codes known as Barker Codes which have a peak-to-sidelobe ratio equal to N [22]. It is of note that methods for sidelobe suppression, including the use of Golay Codes [23], could also be employed. While here we exploit a Barker Code of length $N = 5$, there are many known phase codes – some of which have arbitrarily high N [22].

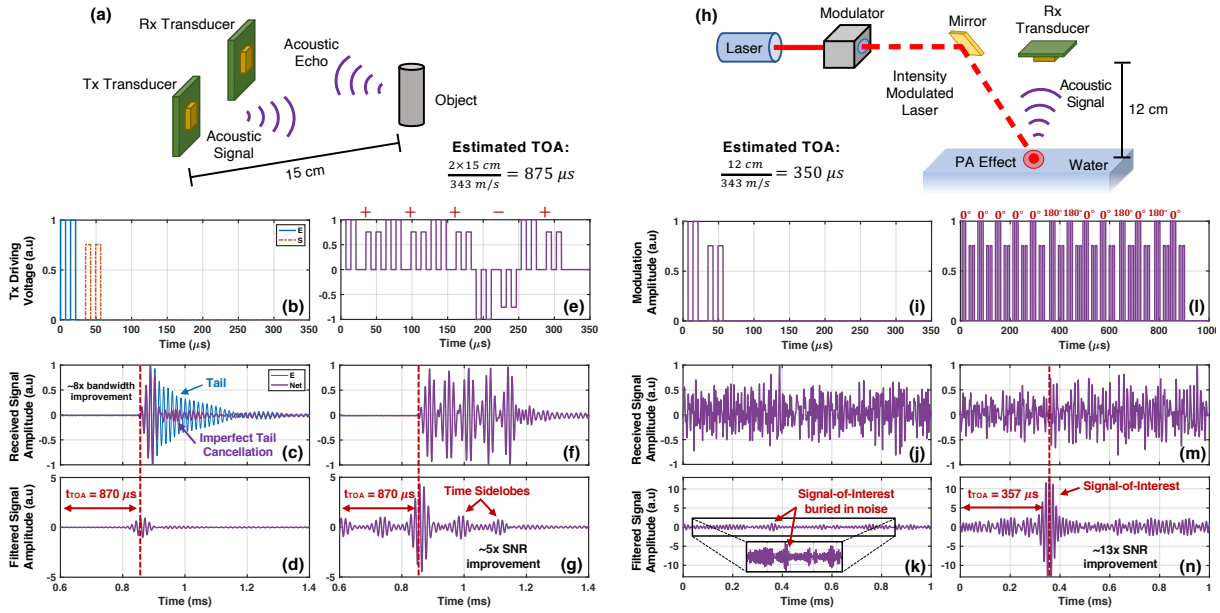

Fig. 4. (a) Experimental setup for US ranging, (b) Transmitter drive voltage waveform with corresponding (c) Received signal and (d) Matched filtered signal, (e) $N = 5$ Barker Code drive signal with corresponding (f) Received signal and (g) Matched filtered signal. (h) Experimental setup for PA measurement, (i) Intensity modulation waveform with corresponding (j) Received signal and (k) Matched filtered signal, (l) $N = 13$ Barker Code modulation waveform with corresponding (m) Received signal and (n) Matched filtered signal.

Whereas transmitting transducers permit negative driving voltage such that the signal in Fig. 3**d** can be directly applied to the transducer, the acoustic signal generated in TA/PA imaging is instead dependent on the envelope of the EM power [24]. Since negative EM power is infeasible, a variant of the driving signal can be derived and employed as shown in Fig. 3**g-i**.

IV. Experimental Results

A. Ultrasound Ranging

To demonstrate the efficacy of the proposed nested phase modulated waveform for use in airborne US applications, we use the experimental setup shown in Fig. 4**a**. The receiving transducer has a frequency response that closely matches that assumed in the simulations above. First, we drive the transmitter with the signal shown in Fig. 4**b**. The corresponding raw received signal and matched filtered signal are shown in Fig. 4**c-d**. Note that the tail cancellation is imperfect due to a mismatch between the modeled and true transducer frequency response. Next, we drive the transmitter with the signal shown in Fig. 4**e** for which the raw received signal and matched filtered signal are shown in Fig. 4**f-g**. Using the proposed modulation, we see a 4.5$\times$ increase in SNR but with equivalent main lobe width to that shown in Fig. 4**d**. While theory predicts a 5$\times$ increase in SNR, this discrepancy is again a result of mismatch between the modeled and true transducer frequency response. A more precise transducer model could be characterized to close the gap between theory and experiment.

B. Photoacoustic Measurement

As discussed above, an acoustic signal generated through the TA/PA effect can be controlled via the envelope, or intensity modulation, of the EM power. To demonstrate that the proposed technique translates through the TA/PA effect, we use the experimental setup shown in Fig. 4**h** where the intensity modulation is performed using an acousto-optic modulator [25]. As seen in Fig. 4**i-n**, the proposed nested phase modulated waveform can also be successfully used in TA/PA imaging applications. For the PA measurement, we adjust the laser power such that the measurement is low SNR and use a longer Barker Code ($N = 13$) to further draw attention to the potential gain in SNR when using the proposed nested phase modulation. Note that even further SNR improvement could be possible by using phase sequences with higher N.

V. Conclusion

Air-coupled US sensing and imaging applications are often SNR constrained requiring that the receiving transducers be sensitive to weak acoustic signals. A transducer's geometry can be optimized prior to fabrication to increase sensitivity at the expense of device bandwidth. Whereas this geometric tuning is fixed to operate at a specific point in the sensitivity versus bandwidth tradeoff space, our technique permits dynamic tunability of sensitivity and bandwidth by modifying parameters of the proposed nested phase modulation. While herein we specifically discuss CMUTs, this technique could be widely applicable across transducer types.

Acknowledgment

The authors would like to thank Prof. B. T. Khuri-Yakub and his research group for the design and fabrication of the utilized CMUTs.

REFERENCES

[1] R. Stoessel, N. Krohn, K. Pfleiderer, and G. Busse, "Air-coupled ultrasound inspection of various materials," *Ultrasonics*, vol. 40, no. 1-8, pp. 159–163, 2002.

[2] W. Grandia and C. Fortunko, "NDE applications of air-coupled ultrasonic transducers," in *1995 IEEE Ultrasonics Symposium. Proceedings. An International Symposium*, vol. 1. IEEE, 1995, pp. 697–709.

[3] P. Pallav, D. A. Hutchins, and T. Gan, "Air-coupled ultrasonic evaluation of food materials," *Ultrasonics*, vol. 49, no. 2, pp. 244–253, 2009.

[4] G. Allevato, J. Hinrichs, M. Rutsch, J. P. Adler, A. Jäger, M. Pesavento, and M. Kupnik, "Real-Time 3-D Imaging Using an Air-Coupled Ultrasonic Phased-Array," *IEEE Transactions on Ultrasonics, Ferroelectrics, and Frequency Control*, vol. 68, no. 3, pp. 796–806, 2020.

[5] N. Gageik, P. Benz, and S. Montenegro, "Obstacle detection and collision avoidance for a UAV with complementary low-cost sensors," *IEEE Access*, vol. 3, pp. 599–609, 2015.

[6] D. Bank and T. Kampke, "High-resolution ultrasonic environment imaging," *IEEE transactions on robotics*, vol. 23, no. 2, pp. 370–381, 2007.

[7] T. Dahl, J. L. Ealo, H. J. Bang, S. Holm, and P. Khuri-Yakub, "Applications of airborne ultrasound in human–computer interaction," *Ultrasonics*, vol. 54, no. 7, pp. 1912–1921, 2014.

[8] A. Golard and S. S. Talathi, "Ultrasound for Gaze Estimation—A Modeling and Empirical Study," *Sensors*, vol. 21, no. 13, p. 4502, 2021.

[9] R. J. Przybyla, H.-Y. Tang, S. E. Shelton, D. A. Horsley, and B. E. Boser, "12.1 3D ultrasonic gesture recognition," in *2014 IEEE International Solid-State Circuits Conference Digest of Technical Papers (ISSCC)*. IEEE, 2014, pp. 210–211.

[10] A. Singhvi, B. Ma, J. D. Scharwies, J. R. Dinneny, B. T. Khuri-Yakub, and A. Arbabian, "Non-contact thermoacoustic sensing and characterization of plant root traits," in *2019 IEEE International Ultrasonics Symposium (IUS)*. IEEE, 2019, pp. 1992–1995.

[11] A. Fitzpatrick, A. Singhvi, and A. Arbabian, "An airborne sonar system for underwater remote sensing and imaging," *IEEE Access*, vol. 8, pp. 189 945–189 959, 2020.

[12] K. C. Boyle, H. Nan, N. Apte, A. Unlugedik, M. S. Aliroteh, A. Bhuyan, A. Nikoozadeh, B. T. Khuri-Yakub, and A. Arbabian, "Non-contact thermoacoustic imaging of tissue with airborne ultrasound detection," in *2015 IEEE International Ultrasonics Symposium (IUS)*. IEEE, 2015, pp. 1–4.

[13] A. Singhvi, K. C. Boyle, M. Fallahpour, B. T. Khuri-Yakub, and A. Arbabian, "A microwave-induced thermoacoustic imaging system with non-contact ultrasound detection," *IEEE transactions on ultrasonics, ferroelectrics, and frequency control*, vol. 66, no. 10, pp. 1587–1599, 2019.

[14] B. Ma, K. Firouzi, K. Brenner, and B. T. Khuri-Yakub, "Wide bandwidth and low driving voltage vented CMUTs for airborne applications," *IEEE transactions on ultrasonics, ferroelectrics, and frequency control*, vol. 66, no. 11, pp. 1777–1785, 2019.

[15] X. Zhang, F. Y. Yamanery, O. Adelegan, and Ö. Oralkan, "Design of high-frequency broadband CMUT arrays," in *2015 IEEE International Ultrasonics Symposium (IUS)*. IEEE, 2015, pp. 1–4.

[16] O. Oralkan, A. S. Ergun, C.-H. Cheng, J. A. Johnson, M. Karaman, T. H. Lee, and B. T. Khuri-Yakub, "Volumetric ultrasound imaging using 2-D CMUT arrays," *IEEE transactions on ultrasonics, ferroelectrics, and frequency control*, vol. 50, no. 11, pp. 1581–1594, 2003.

[17] N. Apte, K. K. Park, A. Nikoozadeh, and B. T. Khuri-Yakub, "Bandwidth and sensitivity optimization in CMUTs for airborne applications," in *2014 IEEE International Ultrasonics Symposium*. IEEE, 2014, pp. 166–169.

[18] N. Apte, K. K. Park, and B. T. Khuri-Yakub, "Experimental evaluation of CMUTs with vented cavities under varying pressure," in *2013 IEEE International Ultrasonics Symposium (IUS)*. IEEE, 2013, pp. 1724–1727.

[19] M. N. Senlik, S. Olcum, H. Köymen, and A. Atalar, "Bandwidth, power and noise considerations in airborne CMUTs," in *2009 IEEE International Ultrasonics Symposium*. IEEE, 2009, pp. 438–441.

[20] A. Singhvi, A. Fitzpatrick, and A. Arbabian, "Resolution Enhanced Non-Contact Thermoacoustic Imaging using Coded Pulse Excitation," in *2020 IEEE International Ultrasonics Symposium (IUS)*. IEEE, 2020, pp. 1–4.

[21] B. R. Mahafza, *Radar systems analysis and design using MATLAB*. Chapman and Hall/CRC, 2005.

[22] M. A. Richards, J. Scheer, W. A. Holm, and W. L. Melvin, "Principles of modern radar," 2010.

[23] M. Golay, "Complementary series," *IRE transactions on information theory*, vol. 7, no. 2, pp. 82–87, 1961.

[24] H. Nan and A. Arbabian, "Coherent frequency-domain microwave-induced thermoacoustic imaging," in *2014 IEEE MTT-S International Microwave Symposium (IMS2014)*. IEEE, 2014, pp. 1–4.

[25] N. A. Riza, *Photonic Signals and Systems: An Introduction*. McGraw Hill Professional, 2013.